Electro-Fenton catalyzed with magnetic chitosan beads for the removal of Chlordimeform insecticide

Soumaya Rezgui[a,b,c,*], Abdeltif Amrane[a], Florence Fourcade[a], Aymen Assadi[a], Lotfi Monser[b,c], Nafaa Adhoum[c]

[a] Ecole Nationale Supérieure de Chimie de Rennes, CNRS, UMR 6226, 11 allée de Beaulieu, CS 50837, 35708 Rennes Cedex 7, France
[b] Institut National des Sciences Appliquées et de Technologie, B.P. No 676, 1080 Tunis Cedex, Tunisia
[c] Unité de Recherche en Eléctrochimie, Matériaux et Environnement (UR16ES02), IPEIK, Université de Kairouan, Kairouan, Tunisia

ARTICLE INFO

ABSTRACT

The degradation of chlordimeform (CDM) has been investigated by a heterogeneous electro-Fenton process involving magnetite supported chitosan beads (Fe_3O_4-Cs) as catalyst. The catalyst was prepared by dropwise addition of an acidic chitosan-metal salts solution into sodium hydroxide precipitation bath. SEM, XRD and FTIR analysis were used to characterize the catalysts. The effect of experimental parameters, such as the current intensity, the amount of iron on chitosan beads, the concentration of the catalyst and the initial pH on the pollutant removal rate was investigated. The optimal conditions for the degradation of 37.5 mg L^{-1} initial CDM concentration were achieved at an applied cathodic current of −5 mA, using 0.5 g L^{-1} of magnetic chitosan beads (with an average iron amount of 0.104 mmol) and at pH = 3. Under these conditions, CDM was effectively removed within 30 min with 80% of NPOC removal after 6 h of treatment. The reaction followed a pseudo-first order kinetic equation. The adsorption test on the chitosan beads (with and without iron) demonstrated that the insecticide removal was solely induced by heterogeneous electro-Fenton treatment with Fe_3O_4-CS beads. In addition, the reusability of this catalyst was effectively demonstrated. Finally, LC–MS analysis allowed the proposal of a plausible degradation route.

1. Introduction

Among all hazardous organic compounds found in wastewater, pesticides occupy an important place due to their high consumption in both agriculture and veterinary to control, repel and prevent pests [1,2]. Pesticides are known as long-term recalcitrant and very toxic compounds [3–5]; their removal from wastewater has become a challenge.

Chlordimeform *N-(4-chloro-o-tolyl)-N,N-dimethylformamidine* (CDM) is a formamidine insecticide/acaricide used on crops, livestock, and pets [6]. CDM is used extensively on fruits and cotton. Its insecticidal action is caused by activation of octopamine receptors, and its toxicity in mammals is mediated by activation of alpha$_2$-adrenergic receptors. CDM is well absorbed and rapidly metabolized to compounds of higher toxicity. Demethylated CDM has a higher acute toxicity and higher affinity for alpha$_2$-adrenoceptors, whereas 4-chloro-*o*-toluidine has carcinogenic properties [7].

The chemical structure of CDM is shown in Fig. 1. Insecticidal formamidines, including CDM have adverse effects on human health and the environment. Toxicological tests carried out on animals at the laboratory scale showed that a long exposure to CDM can primarily affect the cardiovascular system [8]. This insecticide/acaricide can cause profound changes on the visual function [9]. Furthermore, CDM is documented as human and animal carcinogen [7,10]. For these reasons, the application of CDM has been banned in many countries [11,12]. However the detection of CDM residues in human adipose tissue, food and environment was reported in recent studies [13–17].

In the last decades, the Fenton process has been widely employed in the degradation of many persistent organic pollutants [18]. It is based on the oxidation of ferrous ions to ferric iron by hydrogen peroxide according to reaction 1. Hydroxyl radicals ($\cdot OH$) are one of the most stronger oxidants ($E°(\cdot OH/H_2O) = 2.8$ V vs.SHE (StandardHydrogen Electrode)), are non-selective and highly reactive with organic and inorganic compounds [19].

$$Fe^{2+} + H_2O_2 \rightarrow Fe^{3+} + OH^- + \cdot OH \tag{1}$$
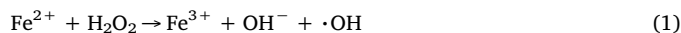
Electrochemical Advanced Oxidation Processes (EAOPs) based on the Fenton's reaction, such as the electro-Fenton (EF) process, have
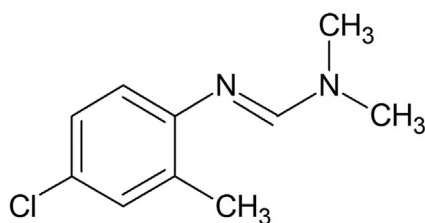

Fig. 1. Chlordimeform molecule.

attracted a great interest due to the in-situ production of hydrogen peroxide using various cathode materials such as carbon felt [20–22], tubular carbon nanotube [23], BDD plate [24], graphite [25] and activated carbon fiber [26]. The hydrogen peroxide is produced in an aqueous medium by the reduction of dissolved oxygen by an electro-Fenton process (Eq. (2)).

$$O_2 + 2H^+ + 2e^- \rightarrow H_2O_2 \tag{2}$$

Hence, the electro-Fenton solves the problems of transportation and storage of this compound, which is expensive, unstable and potentially harmful.

On the other hand, to avoid problems related to the loss of dissolved iron and the production of solid sludge, recent investigations focused on the possibility of using heterogeneous catalysts [27–31]. For this purpose, magnetite Fe_3O_4 has attracted a great attention as efficient catalyst for the heterogeneous Fenton process due to its simple handling, ease of recovery with an external magnetic field, oxidative stability, biological compatibility, strong superparamagnetic behavior and its high catalytic activities [32–34]. The Fenton activity is due to the special structural characters of magnetite which has a cubic inverse spinel structure with tetrahedral and octahedral sites filled by Fe(II) and Fe(III) cations. The catalytic activity is mainly due to the octahedral cations which are almost exclusively exposed on the surface. The octahedral sites are occupied by both Fe(II) and Fe(III), allowing the Fe species to be reversibly oxidized and reduced while keeping the same structure [35,36]. However, the use of Fe_3O_4 NPs can cause the problem of nanoparticles aggregation and the rapid degradation of magnetite onto a given biological matrix [37]. These problems can be overcome by preparation of a hybrid biocomposite using biopolymers as support.

Advantageous alternative supports including biopolymers and biomass-related polymers have been recently employed for the preparation of supported NPs. Biopolymers, such as chitosan and alginate, are indeed attractive candidates to be employed as supports for catalytic applications. They offer several advantages compared to traditional supports including low toxicity and cost, high biocompatibility, availability and abundance [38].

In the last few years, chitosan (CS) has attracted researchers' attention as a natural chelating agent for use in chemical catalysts due to its strong affinity to transition metals, its high sorption capacity, stability of metal anions and physical and chemical versatility [39,40].

The use of appropriate supports to avoid nanoparticles aggregation, as well as the production of supported nanoparticles with higher homogeneous dispersion remains a scientific challenge as attested by the numerous recent studies dealing with this subject [38,41]. Therefore, the aim of this study was to develop highly homogeneous magnetic chitosan beads with a good catalytic activity and stability for CDM insecticide removal by the electro-Fenton process.

2. Experimental set up

2.1. Chemicals products

All chemicals used were of analytical grade and used without further purification. Chlordimeform, sodium hydroxide (NaOH) and magnetite Iron (II,III) oxide Fe_3O_4 were obtained from Sigma-Aldrich

(France). Acetic acid was obtained from Acros Organics (France). Ferrous sulfate Iron (II) ($FeSO_4 \cdot 7H_2O$) was purchased from Prolabo (France). Iron (III) chloride ($FeCl_3 \cdot 6H_2O$) and sodium sulfate decahydrate were from Acros Organics. Sulfuric acid and nitric acid were supplied by Carlo Erba. acetonitrile (HPLC-grade) was purchased from Fisher Scientific (Loughborough, UK). Ultra-pure water obtained from ELGA Purelab Option-Q DV 25 system was utilized for the preparation of all working solutions, as well as HPLC and LC–MS/MS mobile phases.

2.2. Electrochemical process

The electrochemical heterogeneous Fenton reaction was performed in an undivided closed glass cell. The EF process was conducted in galvanostatic mode. The applied current was provided by a power supply Micolab Micronic System (Villetted'anthon, Fr), and the current was controlled and frequently regulated. The cathode was a carbon felt piece (1.5 cm length, 1 cm width, 0.5 cm thickness) and the anode was a platinum wire. The hydrogen peroxide H_2O_2 was produced electrochemically by continuously bubbling compressed air near the cathode leading to the reduction of dissolved oxygen (DO) in acidic solutions containing dilute supporting electrolyte. The pH was adjusted by addition of dilute solutions of sulfuric acid or sodium hydroxide. The ionic strength was maintained constant by the addition of an inert supporting electrolyte (0.05 M, Na_2SO_4). Prior to the electrolysis, compressed air was bubbled for 15 min through the aqueous solutions. Samples were regularly taken to measure the insecticide concentration.

2.3. Analytical procedures

2.3.1. Non-purgeable organic carbon (NPOC) measurements

The mineralization of the chlordimeform was monitored by measuring the non-purgeable organic carbon (NPOC) abatement by TOC-VCPH/CPN Total Organic Carbon Analyzer Schimadzu.

2.3.2. HPLC analysis

The measurements of the residual CDM concentration were performed by a Waters High Performance Liquid Chromatography (HPLC) system consisting of a Waters™ 600 instrument, equipped with a C18 reverse-phase Column (4.6 mm × 250 mm, 5 μm), along with a 996 Photodiode array detector and a Waters 717 plus Autosampler injector. The system was controlled through an Empower program. Prior to analysis, the samples had to be filtered through a 0.45 μm filter. The injection volume was set at 50 μL and an isocratic eluent Water/Acetonitrile (60/40) was pumped at a flow rate of 1 mL min^{-1}. CDM had a retention time of 10 min under these conditions and many peaks of the byproducts appeared at lower retention times. Detection was performed with a photodiode array detector Waters 996 at 240 nm.

The detection and evolution of carboxylic acids was followed by an ion exclusion chromatography system Dionex DX120. A system equipped with a column Dionex AS11-HS (4 × 250 mm) coupled to a conductivity detector was used. Separation was achieved by a gradient elution composed of a mixture of potassium hydroxide (KOH) and water, as follows: 0–10 min (isocratic 10 mM); 10–25 min (gradient from 10 to 45 mM); 25–35 min (isocratic 45 mM). Flow rate was adjusted to 1 mL min^{-1}. The injection volume was set at 250 μL. The system was connected with an acquisition and data treatment unit commanded by analytical Chromeleon SE software.

The determination of inorganic anions was carried out by an ion chromatography system (IC-861, Metrohm) equipped with an AS4A-SC column (150 mm × 4 mm). The eluents were Na_2CO_3 (3.2 mM) and $NaHCO_3$ (1 mM) solutions pumped at a flow rate of 0.7 mL min^{-1} and a pressure of around 2000 psi.

2.3.3. UPLC–MS/MS analysis

The degradation intermediates were identified through LC–MS/MS ultra-high pressure liquid chromatography (Acquity UPLC – Waters)
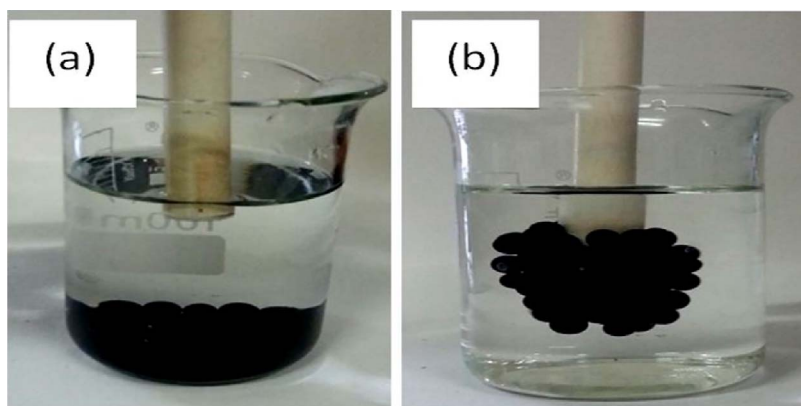
coupled to a Waters Micromass Quattro Premier (Waters Corporation, Manchester, UK) triple quadruple mass spectrometer as detector. It was operating with an electrospray source in positive ionization mode with a cone potential of 25 V. Analyses were performed in full scan and daughter scan modes, with a collision energy of 25 eV. Spectra were acquired between 80 and 500 m/z and the data were treated with Micromass Mass-Lynx 4.1 software. The UPLC system (Waters Corporation, Milford, MA, USA) consists of an Acquity UPLC binary solvent manager, an Acquity UPLC sample manager and an Acquity UPLC column heater equipped with a Waters Acquity UPLC BEH Shield RP18 column (2.1 mm × 100 mm, 1.7 mm particle size) (Milford, MA, USA) maintained at 45 °C. Analyses were performed using 0.1% formic acid in acetonitrile as eluent A and 0.1% formic acid in a mixture of MilliQ Water/Acetonitrile (90/10, v/v) as eluent B, delivered at a flow rate of 0.4 mL min^{-1}. The elution gradient started with 100% of eluent B. After 1 min, the proportion of eluent A increased linearly to 100% of A within 8 min.

2.3.4. Determination of the iron content

The amount of iron in the catalyst, as well as, the total leached iron was determined by atomic absorption spectrophotometry (AA140, VARIAN) whose detection limit is estimated to 3.1 µmol L^{-1}. For the heterogeneous catalysts, it was necessary to obtain an iron solution by acid leaching samples of Fe$_3$O$_4$-Cs beads in concentrated hydrochloric acid solution until complete discoloration of the bead (after 12 h).

In order to determine the molar ratio Fe^{2+}/Fe^{3+} in Fe$_3$O$_4$-Cs beads, soluble iron quantification was estimated by the standard 1,10-phenantroline spectrophotometric method [42]. 1,10-phenantroline reacted with Fe^{2+} forming a colored complex which can be measured at a wavelength of 510 nm. While the amount of the individual Fe^{3+} was calculated from the difference between the total iron and the Fe^{2+}. The amount of total iron was estimated by the same spectrophotometric method after the addition of a reducing agent of Fe^{3+} to Fe^{2+}.

2.3.5. Determination of the zero point charge of the catalyst

The pH of zero point charge pH$_{zpc}$ was determined by the simple method of salt addition [43]. A series of 5 suspensions were prepared by mixing 40 mL of sodium nitrate NaNO$_3$ (0,1 M) with 0.2 g of sample. The pH of each solution in the series of NaNO$_3$ was beforehand adjusted to 2, 6, 8, 10 and 12 using a diluted HNO$_3$ or NaOH solution. Then, each flask was vigorously agitated for 24 h. The final pH was measured. After this time each resulting pH was measured and the initial pH (pH$_0$) vs. the difference between the initial and final pH values (ΔpH) was plotted. The pH$_{zpc}$ was taken as the point where ΔpH = 0.

2.3.6. Morphology of the beads

Surface morphology was characterized on a field-emission scanning electron microscope (SEM). SEM was performed on a field effect JEOL JSM-6301F instrument equipped with an EDS Oxford Inca Energy 300 SEM at an accelerating voltage of 15 kV.

2.3.7. FTIR and XRD analysis

Catalysts and virgin chitosan beads were characterized using a FTIR model spectrum 100 (PerkinElmer, USA) with a wavelength run of 4000–400 cm^{-1}. For the same samples, XRD measurements were carried out using X'Pert PRO MPD X-ray diffractometer (PANalytical) with monochromatic Cu-Kα radiation source (λ = 1,5418 Å).

2.4. Preparation of magnetic chitosan beads

The chitosan used in the current work was extracted from shrimp shell waste according to the preparation method detailed by Islam et al. [44]. Shrimp shells were collected from the central market of Tunis.

2.4.1. One-step method for the preparation of magnetic chitosan gel beads (The in-situ method)

The in-situ formation of magnetic particles in polymer matrix can be obtained by the alkaline co-precipitation of ferric and ferrous salts [45]. For the synthesis of magnetic chitosan gel beads, Fe^{3+}:Fe^{2+} in the molar ratio 2:1 were added to 2% chitosan dissolved in acetic acid solution 1%. The gel solution was mixed by constant stirring for 1 h to obtain an orange homogeneous gel solution. Then, the mixture was dropped through a syringe into a hardening solution of sodium hydroxide (1 M) to create spherical and uniform chitosan gel beads which have magnetic properties (Figs. 2 and 3). In contact with NaOH solution, the dark color of the beads indicates the in-situ precipitation of iron oxide. Nanoparticles of metal oxides, in particular, magnetite Fe$_3$O$_4$ and maghemite Fe$_2$O$_3$ are often synthesized by the alkaline co-precipitation of ferric and ferrous salts. [46].

The obtained particles were washed with deionized water for several times until pH reached a constant value (≈ 6). Then, the prepared beads were dried at room temperature.

2.4.2. Method 2: the mixing of pre-formed polymer and magnetic particles (The ex-situ method)

For comparison, magnetic chitosan beads Fe$_3$O$_4$-Cs was prepared by deposition of magnetite (Fe$_3$O$_4$) at the surface of chitosan gel beads. Chitosan beads were prepared by the previously described method without the addition of iron. Thereafter, prepared particles were introduced into 1% magnetite suspension. The mixture was stirred for 12 h using an incubator shaker (innova$^{@}$40).
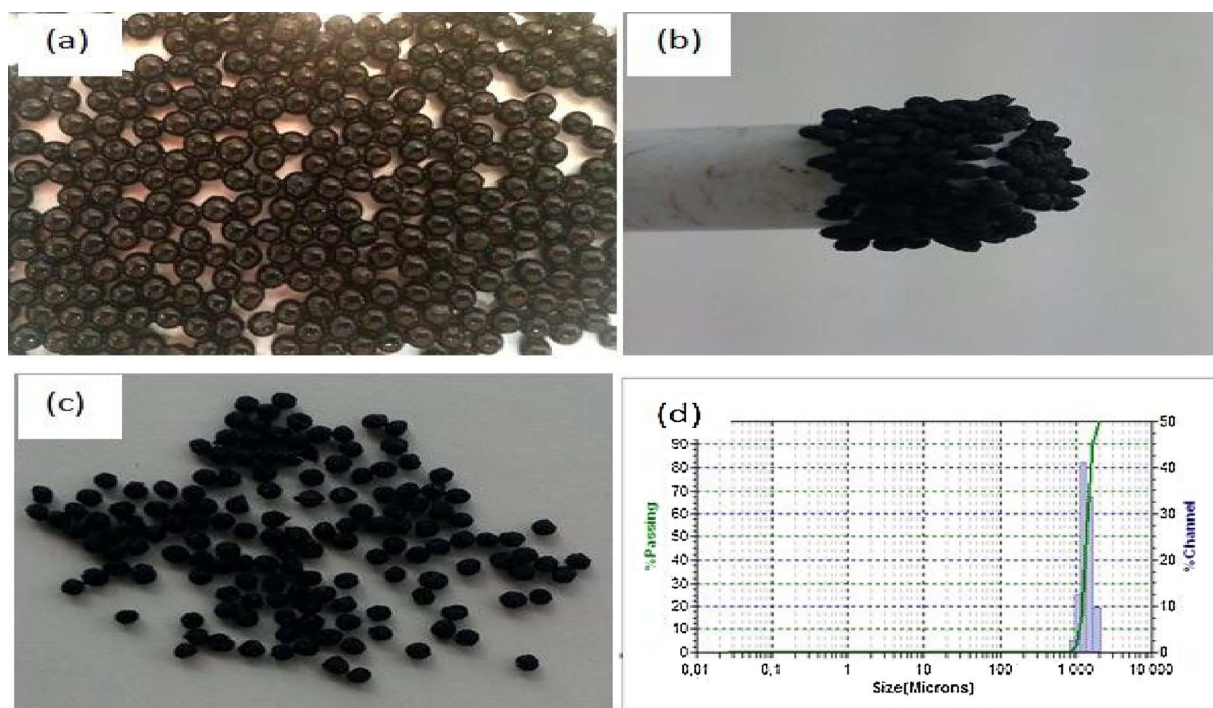
Fig. 3. Digital photographs of the magnetic chitosan beads prepared by the approach in-situ: (a) wet beads; (b) dry beads with external magnetic field; (c) dry beads without external magnetic field (d) The schematic of laser diffractometry measurement for Fe_3O_4-Cs beads.

3. Results and discussion

3.1. Structural and textural characterization of the catalyst

3.1.1. Principle of in-situ preparation of magnetite nanoparticles in chitosan matrix

The main advantage of the in-situ approach is the synthesis of the nanosized magnetite and the solidification of chitosan beads in the alkaline co-precipitation bath. This occurs in one step and can be described according to the following reaction:

$$CS-NH_3^+ + Fe^{2+} + 2Fe^{3+} + 8OH^- \rightarrow CS-NH_2 + FeO.Fe_2O_3 + 4H_2O \quad (3)$$
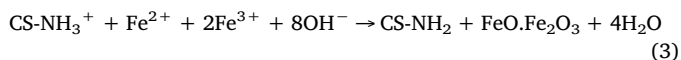
As explained by Wang [47], ferric and ferrous ions are chelated by amino groups of chitosan in the prepared mixture CS/iron salts gel solution. Then, in contact with hydroxide ions the chelated ferrous and ferric ions [(chitosan-NH_2)$_2$–Fe^{2+}, (chitosan-NH_2)$_2$–Fe^{3+}] provide nucleation site for magnetite crystals. Thus, Fe_3O_4 and chitosan would be precipitated at the same time. The scheme of the in-situ preparation principle of magnetite in chitosan matrix is presented in Fig. 4.

This way of preparation is more advantageous than that involving magnetite powder, since it allows a better homogenization of the solution and thus minimizes the loss of magnetic material during the preparation procedure [48]. The homogeneous distribution of metal oxide in the catalyst is due to the uniform distribution of amino groups in the chitosan matrix. Therefore, formed metal nanoparticles are strongly bound to chitosan by combination with a wide number of active sites of the polymer [49]. In fact, in the in-situ approach, the polymer is involved in the synthesis of metal oxide nanoparticles; it has therefore a positive impact on their stabilization and their isolation reduces the problem of aggregation. This can enhance the catalytic performance of prepared magnetic chitosan beads.

To highlight the effect of iron concentration on the textural proprieties of the catalyst, the amount of iron added to chitosan gel solution (2%) was varied from 5 to 15 mmoL per 1 g of chitosan flakes. The obtained catalysts were characterized by SEM image, XRD and FTIR analysis.

3.1.2. Morphology and bead size measurements

For the in-situ approach, the morphology of the beads surface and the core observed by SEM micrographs (Fig. 5) after drying demonstrated that, for high concentrations of iron (≥ 10 mmoL of iron/1 g of CS) (Fig. 5a and b), beads have an elongated spherical form with a rather smooth surface. For a low concentration of iron ($= 5$ mmoL of iron/1 g of CS) (Fig. 5c), the bead loses its spherical shape and its surface became crumpled.

For these catalysts, wet beads had a spherical form. After drying, beads with a high amount of iron retained their spherical shape. In contrast, beads with a low amount of iron showed an empty pocket structure similar to that found by Xiaopeng Xiong et al. who explained this result by the shrinkage of the particles by removal of the inside water during drying [50].

Besides, the difference between the surface of chitosan without and with the deposit of Fe_3O_4 nanoparticles was obvious in Fig. 5d and e respectively; magnetite particles are visible on the surface of Fe_3O_4-Cs beads prepared by the ex-situ approach.

The dried bead size was measured by laser diffractometry using (Mictotrac-S3500) considering the MIE and FRAUNHOFER theory (0.02 μm–2800 μm). For all Fe_3O_4-Cs beads prepared via the in-situ approach, the diameter is still constant, and it is estimated to around 1.3 mm (Fig. 3d). Therefore, the size of beads is not affected by the amount of iron salts added initially to the chitosan gel matrix.

3.1.3. Phase structure of the catalysts

The presence of magnetite (Fe_3O_4) phase was confirmed by XRD analysis of dried CS/Fe_3O_4 beads (in situ synthesis) (Fig. 6). The iron oxide phase was identified from the XRD patterns by the peak positions at 2Theta; $= 30.4°, 35.7°, 43.5°, 53.4°, 57.4°, 63.1°$ and $73.0°$, which can be attributed to the diffraction planes of (220), (311), (400), (422), (511), (440), (533), respectively, for the crystallized structure of the Fe_3O_4.

The mean size of the ferromagnetic particles, prepared in-situ in the beads was 10.2 nm, as calculated by the Scherrer's equation (Eq. (4)).
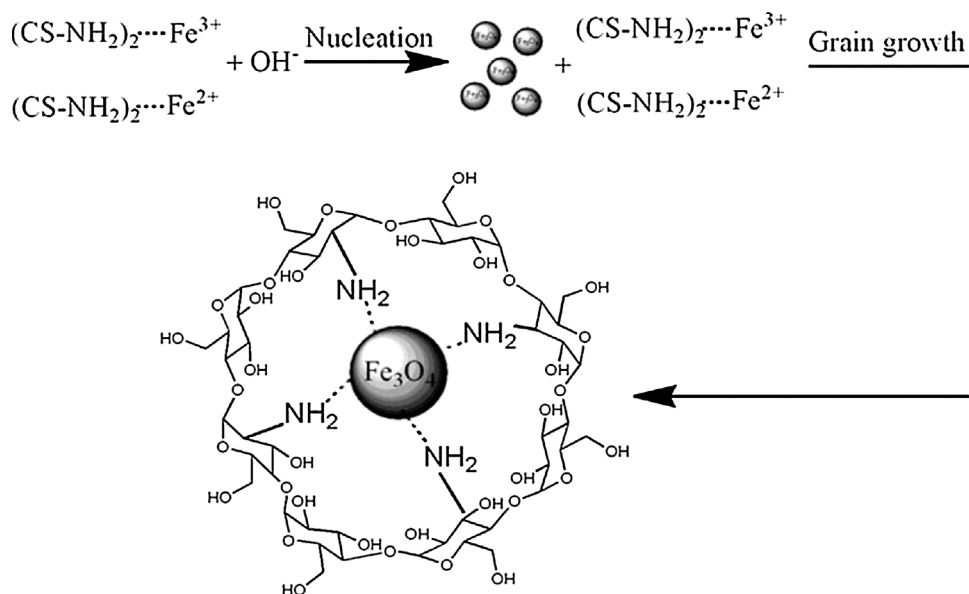
Fig. 4. Principle of in-situ mineralization of magnetite nanoparticles in chitosan hydrogel [37].
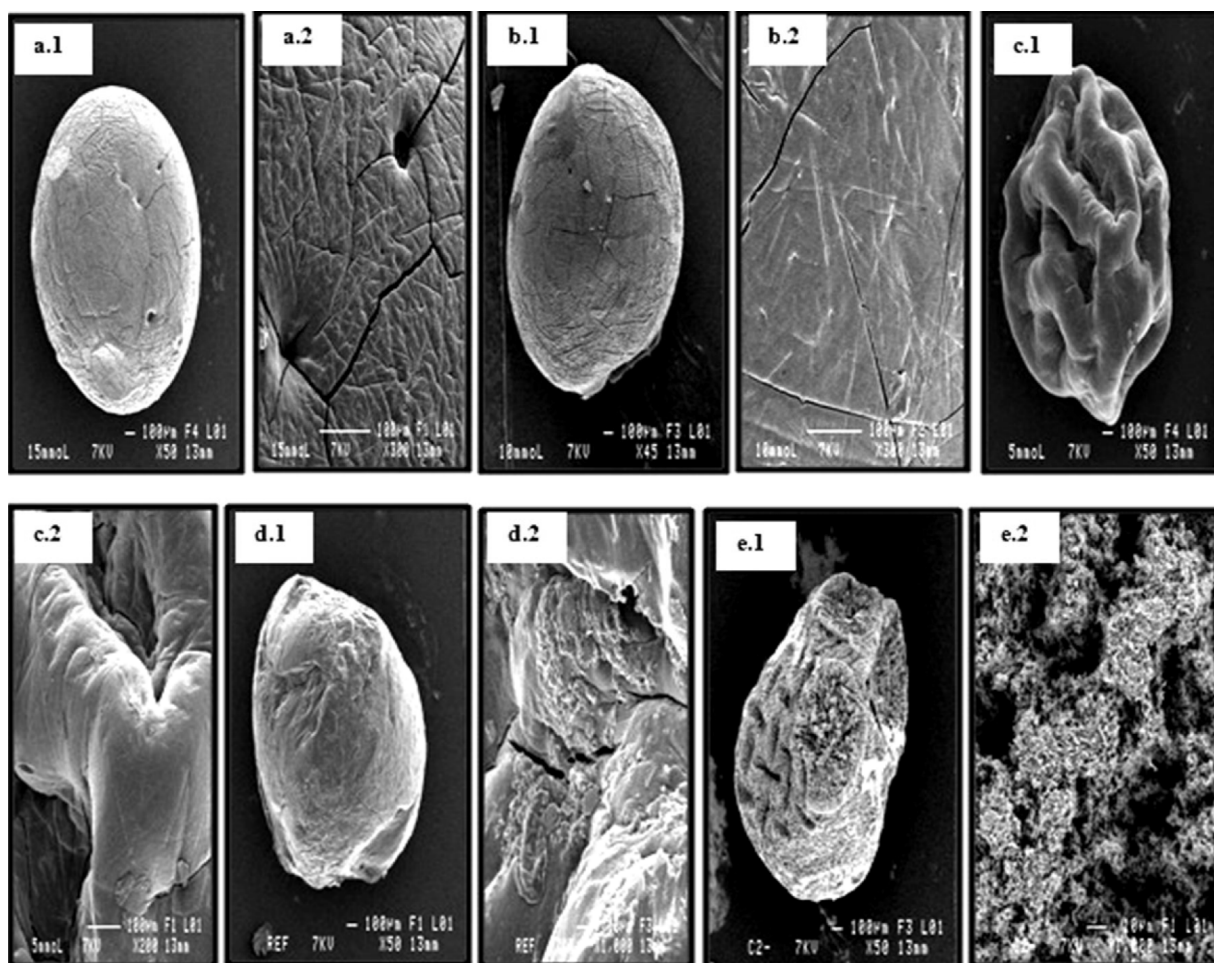

Fig. 5. Morphology of catalysts: (a,b,c) Fe_3O_4-Cs beads prepared via method 1 (a) 15 mmol of Fe/1 g of Cs (b) 10 mmol of Fe/1 g of Cs (c) 5 mmol of Fe/1 g of Cs; (d) virgin chitosan beads; (e) Fe_3O_4-Cs beads prepared via method 2.

$$D = \frac{K \times \lambda}{\beta \times \cos(\theta)} \qquad (4)$$

Where D is the mean size of crystallites (nm), K is a constant related to crystallite shape, normally taken as 0.9, λ is the X-ray wavelength, β is

the full width at half the maximum (radians) of the X-ray diffraction peak and θ is the Bragg angle (deg).

This finding is in agreement with the related literature [51]; the Fe_3O_4 crystals induced by the chitosan hydrogel should have a narrow size distribution and a small diameter due to the restriction of iron ions
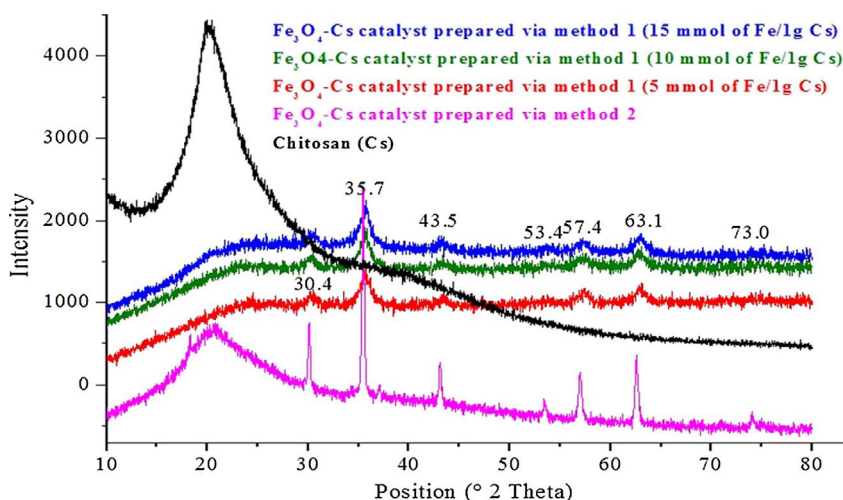
Fig. 6. X-ray powder diffractograms of the prepared magnetic chitosan beads.

by the chelation effect that avoids the crystal growth of magnetite. It has been reported that Fe_3O_4 particles with size lower than 20 nm are superparamagnetic [46]. Therefore, it might be assumed that a part of the magnetite, formed *in situ* in the beads, was in a superparamagnetic state. It means that they are easily attracted by a magnetic field, but retain no residual magnetism at zero magnetic field [52]. The superparamagnetism is an important advantage which provided an additional stability of our catalyst and its dispersion after the application of an external magnetic field.

Furthermore, the size of Fe_3O_4 particles in the magnetic chitosan beads prepared by the ex-situ method was estimated to be 45.3 nm.

3.1.4. FTIR analysis of the catalysts

The deacetylation degree of the prepared chitosan (% DD) was estimated at around 75% and it was evaluated using the Eq. (5) proposed by Brugnerotto et al. [53].

$$\%DD = 100 - [[31.92*(A_{1320}/A_{1420})] - 12.20] \qquad (5)$$

Where A_{1320} and A_{1420} are the values of absorbance relative to baseline that occur in the FTIR spectrum of the extracted chitosan (Fig. 7).

The binding of Fe_3O_4 to chitosan and the effect of the amount of iron in the chitosan matrix were also confirmed by FT-IR analysis. Fig. 7 shows the FT-IR spectra of prepared catalysts and virgin chitosan powders. In the FT-IR spectra of chitosan, the characteristic bands of

NH− and OH− stretching vibrations appeared at 3430 cm^{-1}. The band at 1645 cm^{-1} was attributed to NH bending vibrations. The bands at 1150 cm^{-1} (−OH bending), 1072 cm^{-1} (−C−O−C− stretching vibrations) and 1031 cm^{-1} (−OH bending) were due to the saccharide structure [48].

In the FT-IR spectra of the catalysts, a new band appeared in the low-frequency region (1000–500 cm^{-1}) due to the iron oxide skeleton (−Fe-O− stretching vibration) which confirmed that the precipitation reactions carried out with chitosan produced a composite chitosan-Fe oxide nanoparticles [48,54,55]. By increasing the amount of iron per mass of chitosan, the characteristic band of Fe−O became wide. Compared with the spectrum of chitosan, a slight shift and a significant decrease in the transmittance of the band at 3430 cm^{-1} occurred following iron addition. This indicated the occurrence of metal-NH$_2$ bonds [56,57].

3.2. Degradation of chlordimeform by heterogeneous electro-Fenton process

3.2.1. Effect of the current intensity

A key parameter in the electro-Fenton process is the applied current in two-electrode cells [58–60]. Zhimin Qiang et al. [60] investigated the optimal parameters such as the cathodic potential to improve the Faradic current efficiency of H_2O_2 production. They found that the optimal conditions for H_2O_2 generation are cathodic potential of
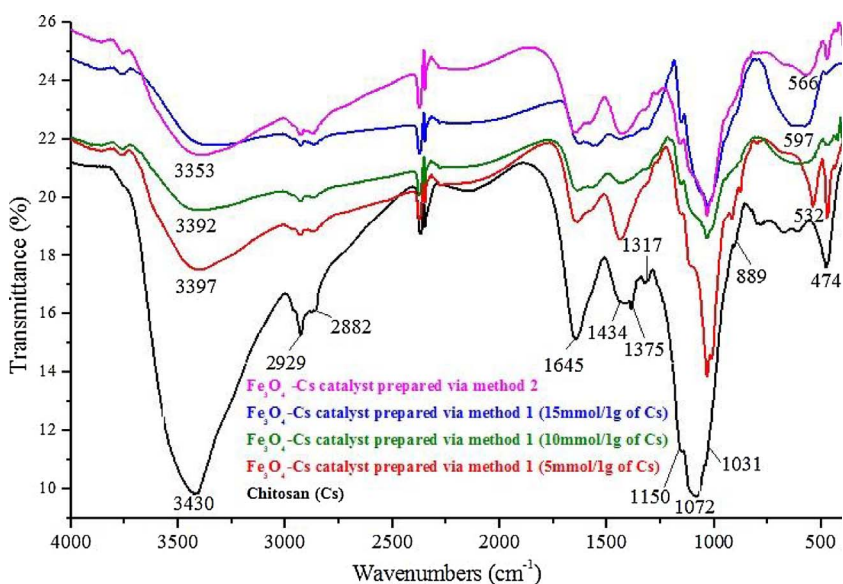
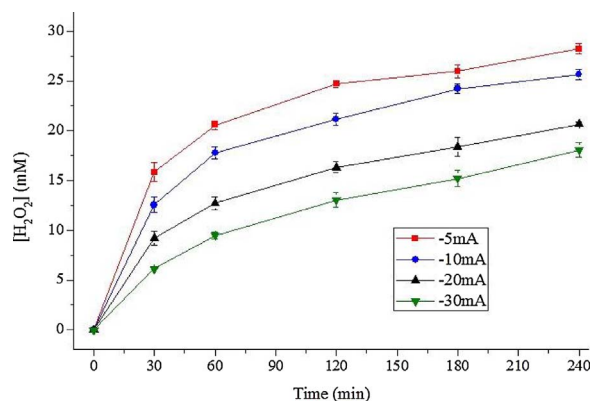**Fig. 7.** FTIR spectra of the used catalysts.

Fig. 8. Effect of the applied cathodic current on the change of accumulated hydrogen peroxide concentration with time during electrolysis of 30 mL of a 0.05 M Na_2SO_4 at pH = 3.

-0.5 V vs. saturated calomel electrode (SCE), with an oxygen mass flow rate of 8.2×10^{-2} mol/min in acidic conditions. In this context, an electrochemical study carried out previously, in our working conditions (data not shown), indicated that -5 mA corresponded to an average current intensity obtained during electrolysis carried out at a constant potential of -0.5 V/EDS.

To confirm the effect of the current intensity on the electrochemical generation of H_2O_2 with the felt carbon cathode, electrolysis was performed in our experimental conditions (30 mL of a 0.05 M Na_2SO_4 solution adjusted to an initial pH = 3 with concentrated H_2SO_4) by applying several cathodic current intensities. Fig. 8 shows the effect of the applied current intensity on the amount of accumulated hydrogen peroxide during 4 h of electrolysis. The hydrogen peroxide concentration was measured by titration with a solution of potassium permanganate $KMnO_4$. As expected, the measured concentration of the oxidant depends on the applied intensity. Final solutions with 18.1 ± 0.7, 20.7 ± 0.2, 25.6 ± 0.6 and 28.2 ± 0.5 mM hydrogen peroxide were obtained, after 4 h of electrolysis, at -30, -20, -10 and -5 mA, respectively. Thus, the maximum hydrogen peroxide concentration was achieved at an applied cathodic current of -5 mA.

Taking into account that the degradation of CDM occurs by the reaction with hydroxyl radicals ·OH produced by the activation of the electro-generated hydrogen peroxide on the actives sites of iron supported on chitosan beads, the rate of pollutant mineralization is directly affected by the amount of electro-generated hydrogen peroxide which is the precursor of this reaction.

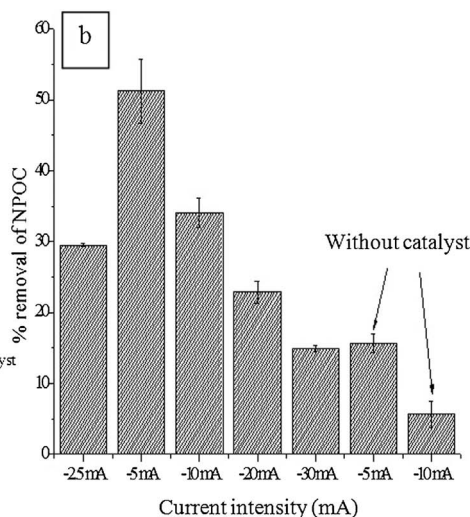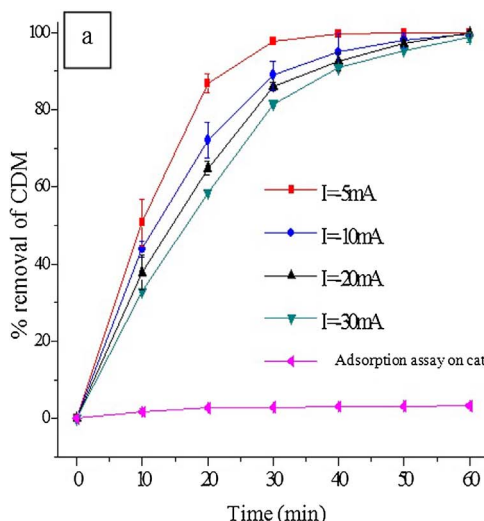These results are confirmed by the study of the impact of the current

intensity on the CDM removal. To this purpose, various current intensities were applied, in the range of -5 mA to -30 mA. Results in Fig. 9a show that changing the applied cathodic current did not lead to a significant increase in the kinetic of degradation of CDM. However, it is clear from Fig. 9b that the change of the applied cathodic current greatly influenced the rate of mineralization because the values of NPOC removal within 4 h of electrolysis decreased from 51.2 ± 4.5% to 14.9 ± 0.5% for decreasing currents values from -5 mA to -30 mA. For higher current intensity, the NPOC removal decreased to 29.5 ± 0.2% for a cathodic current intensity equal to -2.5 mA. In the absence of catalyst, the yields of NPOC removal did not exceed 15.6 ± 1.3% and 5.7 ± 1.9% for I = -5 mA and I = -10 mA, respectively.

From our study, the highest NPOC removal was obtained at an applied current equal to -5 mA, which represents, as discussed above, the optimal applied current for the electro-generation of oxidant species. An applied cathodic current of -5 mA was therefore selected and considered thereafter.

To highlight the contribution of the adsorption process on the removal of the insecticide, the catalyst was introduced into CDM solutions in the absence of current. Results showed that the fraction of CDM adsorbed in magnetic chitosan beads did not exceed 3%. This proves that there was no affinity between the target molecule and the catalyst. This result can be explained by the point of zero charge (pzc) value of the Fe_3O_4-Cs beads which is around pH = 7 (Table 1). Thus, the catalyst surface is positively charged in acidic media (pH < 7), whereas it is negatively charged under alkaline conditions (pH > 7). At pH = 3, the charge of catalyst surface is positive. However, the charge of CDM (pKa = 3.85) is neutral. This accounts for the weak interaction between the pollutant and the catalyst as proved by the adsorption test.

3.2.2. Effect of the amount of iron in chitosan beads

The catalytic activity is influenced by the availability of active sites (iron) on the surface of the catalyst which react, as mentioned previously, with hydrogen peroxide in order to generate hydroxyl radicals [29].To highlight the effect of the iron content on the catalytic properties of magnetic chitosan beads, the amount of iron added initially to the chitosan matrix was varied from 5 to 15 mmol per 1 g of polymer flakes. Iron analysis was carried out by atomic absorption spectroscopy to quantify the amount of metal/mass of catalyst for each sample. The corresponding results are shown in Table.1. It can be noted that for the higher iron content (> 15 mmol of iron/1 g of chitosan), the rigidity of the beads decreased; they could be easily broken by simple magnetic stirring.

Fig. 10 shows the time-courses of CDM removal during the electro-

Fig. 9. Effect of the current intensity: [CDM] = 37.5 mg L^{-1}; pH = 3; The amount of Fe/ mass of catalyst = 0.083 mmol, [catalyst] = 0.5 g L^{-1}.

Table 1
The amount of iron in 15 mg mass of catalyst.

Samples	Fe$_3$O$_4$-Cs beads prepared via method 1 (amount of iron/1 g of Cs)			Virgin Cs	Fe$_3$O$_4$-Cs beads prepared via method 2
	5 mmol	10 mmol	15 mmol		
pH (zpc)	7.2	7.1	7.2	7.2	7
[Fe] (mmoL/mass catalyst)	0.046 ± 0.001	0.083 ± 0.003	0.104 ± 0.001	0	0.0422 ± 0.0008

Fenton reaction. It can be seen that the kinetics of pollutant removal increased with increasing iron concentration and total removal was observed within 60 min as shown in Fig. 10b. The removal of the pesticide was found to follow a pseudo-first order kinetic model with k = 0.072 min^{-1}, 0.110 min^{-1} and 0.160 min^{-1} for 0.046 mmol, 0.083 mmol and 0.104 mmol of iron per 15 mg of catalyst, respectively. The mineralization yields (Table 2) also increased with the mass of iron, from 61.4 ± 2.1% to 79.7 ± 1.7%, for amounts of iron per mass of chitosan increasing from 0.046 mmol to 0.104 mmol, after 6 h of treatment.

To better understand the effect of the amount of iron on the structural and textural properties of magnetic chitosan beads, XRD and FTIR analysis and SEM micrographs were done.

From the diffractogram XRD (Fig. 6), it can be concluded that the catalytic activity increased for higher crystalline structure. However, the crystallinity is a necessary but not the only important factor affecting the catalytic performance. The activity of catalyst is also affected by surface area and the porosity, which could be related to the increase of the amount of active sites available for the reaction. Thus, the highest amount (0.104 mmol) was selected as the optimal amount of iron supported on chitosan beads, ensuring a good stability of the catalyst and a high catalytic activity; it was therefore considered thereafter. As observed above, negligible involvement of pesticide adsorption on the chitosan beads, containing iron or not, was confirmed.

3.2.3. Effect of the catalyst dosage

In heterogeneous systems, the catalyst dosage plays a crucial role since it controls the rate of hydroxyl radicals' production. Thus, it is one

Table 2
Summary table of mineralization rates for each experiment.

Parameter	Essay	% removal of NPOC after 6 h of treatment
The amount of iron per mass of catalyst	0.046 mmol	61.4 ± 2.1
	0.083 mmol	70.1 ± 0.7
	0.104 mmol	79.7 ± 1.7
The catalyst dosage	0.25 g L^{-1}	63.5 ± 0.8
	0.5 g L^{-1}	79.7 ± 1.7
	0.75 g L^{-1}	71.8 ± 1.3
The preparation method of catalyst	In-situ synthesis of Fe$_3$O$_4$ on polymer matrix	79.7 ± 1.7
	Mixing of pre-formed C$_S$ beads and Fe$_3$O$_4$ NPs	37.8 ± 2.3
Type of EF process	Heterogeneous process	79.7 ± 1.7
	Homogeneous process	65.6 ± 4.2
pH	pH = 3	79.7 ± 1.7
	pH = 7	32.7 ± 2.3

of the major parameters to be studied. For this purpose, several experiments were performed with 0.25 g L^{-1}, 0.5 g L^{-1} and 0.75 g L^{-1} of catalyst.

As can be seen when the catalyst dosage increased from 0.25 g L^{-1} to 0.5 g L^{-1}, the percentage of degradation of CDM increased within 30 min from 65.5 ± 2.2% to 99.1 ± 0.9% (Fig. 11), and the rate of NPOC removal after 6 h of treatment increased from 63.5 ± 0.8% to 79.7 ± 1.7% respectively (Table 2), because increasing the accessibility of iron led to an increase of catalytic active sites. However, beyond 0.5 g L^{-1} of catalyst, the CDM removal and the mineralization
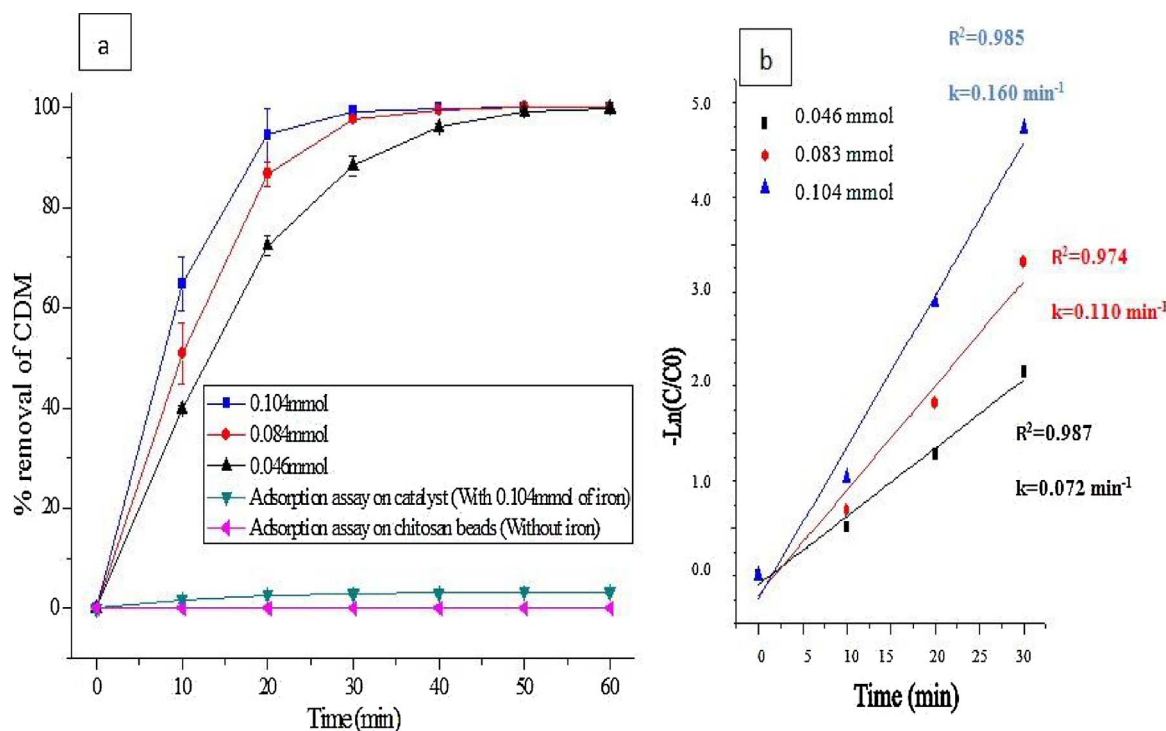

Fig. 10. Effect of the amount of iron supported in chitosan beads: [CDM] = 37.5 mg L^{-1}; pH = 3; [catalyst] = 0.5 g L^{-1}.
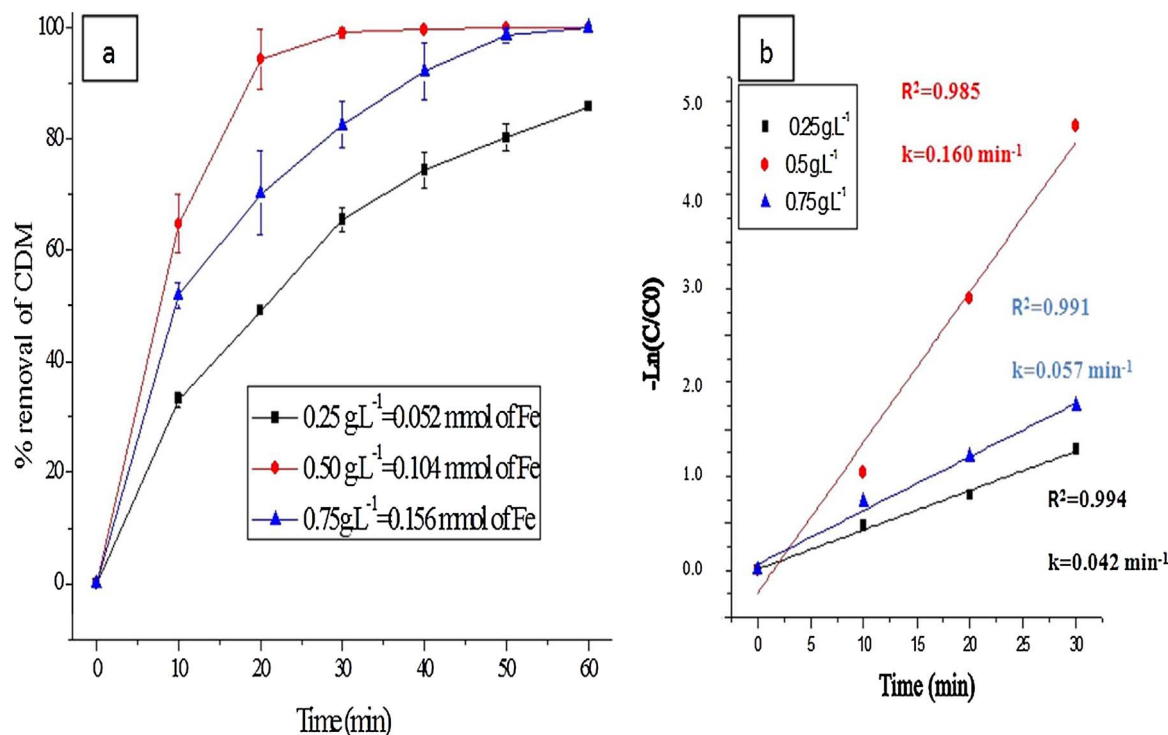
Fig. 11. Effect of the concentration of catalyst: [CDM] = 37.5 mg L^{-1}; pH = 3.

yields decreased to 82.6 ± 4.2% (Fig. 11) and 71.8 ± 1.3% (Table 2), respectively. This can be explained by the reaction of hydroxyl radicals with the excess of active iron sites as shown in Eq. (6).

$$Fe^{2+} + \cdot OH \rightarrow Fe^{3+} + OH^{-} \tag{6}$$

Otherwise, it has been reported that the increase of the catalyst dosage, may reduce the current intensity [28]. In fact, as commonly known, the mass of catalyst can greatly affect the mass transport in the medium which reduce the current intensity.

The degradation of CDM, with the change of catalyst concentration, followed a pseudo first order kinetic as shown in Fig. 11**b**, as found previously in Fig. 10**b**. The kinetic constants were found to be 0.042 min^{-1}, 0.160 min^{-1} and 0.057 min^{-1} for 0.25 g L^{-1}, 0.5 g L^{-1} and 0.75 g L^{-1}, respectively.

From the above results, 0.5 g L^{-1} was the optimal catalyst amount and was therefore considered thereafter.

3.2.4. Comparison of the different preparation methods of Fe3O4-CS beads

Among the classical synthesis methods, detailed by White et al. [38] for the chemical preparation of supported metal nanoparticules on porous materials, two different methods were compared in the present study: The first was the synthesis in situ of the Fe$_3$O$_4$ on a polymer matrix by the co-precipitation method; for comparison, the second method was a simple deposition of Fe$_3$O$_4$ nanoparticles on pre-formed chitosan gel beads surface.

The Fe$_3$O$_4$-Cs beads prepared by the co-precipitation method were found to have a higher catalytic activity: it was observed 99.1 ± 0.9% and 85.4 ± 0.6% CDM removal within 30 min (Fig. 12) and 79.7 ± 1.7% and 37.8 ± 2.3% mineralization after 6 h (Table 2) of electrolysis by the methods 1 and 2, respectively. The first method allowed the incorporation of a considerable amount of magnetite in the beads (0.1039 ± 0.0014 mmol of iron/mass of catalyst) with higher homogeneous dispersion compared to the deposition method of magnetite at the surface of chitosan beads. Indeed, the amount of iron deposited at the surface of Fe$_3$O$_4$-Cs beads prepared via the ex-situ approach was estimated to be 0.0422 ± 0.0008 mmol/mass of catalyst.

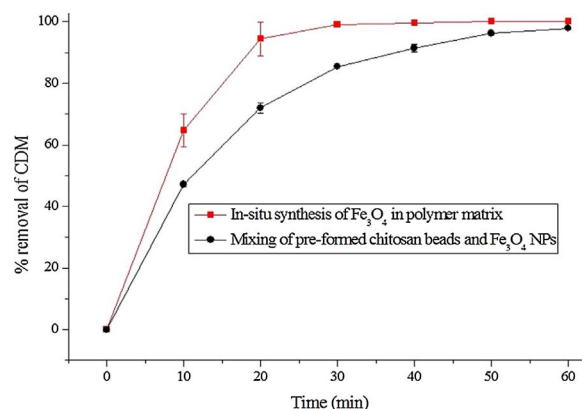Compared to the ex-situ method for the preparation of magnetic

Fig. 12. Effect of the preparation method of catalyst: [CDM] = 37.5 mg L^{-1}; pH = 3 and [catalyst] = 0.5 g L^1.

beads, the in-situ approach was simpler and ensured a spherical and uniform shape (Fig. 5) and a good rigidity of the beads with high magnetic properties. Furthermore, it exhibited, as demonstrated previously, a high catalytic activity. For these reasons, the co-precipitation method of chitosan and magnetic particles was chosen for the preparation of magnetic chitosan beads.

3.2.5. Comparison of the homogeneous and heterogeneous Fenton processes

The degradation of CDM by the electro-Fenton process was studied with the same amount of supported and free iron. The heterogeneous electro-Fenton process was found to be slightly more efficient for the removal of CDM than the homogeneous process (Fig. 13). The difference was clearly more pronounced upon examination of mineralization yields, 79.6 ± 1.1% and 65.6 ± 4.2% for the heterogeneous and homogeneous processes after 6 h of electrolysis, respectively (Table 2). This finding can be attributed to a precipitation of iron(III) in the homogeneous process which causes a reduction of the dissolved iron concentration [28]. Furthermore, homogeneous processes have some disadvantages, such as production of sludge with a high content in iron
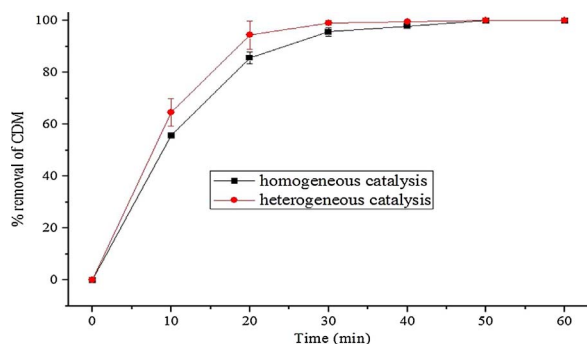
Fig. 13. Comparison of heterogeneous and homogeneous electro-Fenton processes: [CDM] = 37.5 mg L^{-1}; pH = 3; [heterogeneous catalyst] = 0.5 g L^{-1}; [Fe(supported/free)] = 0.1 mmol.

and iron deactivation by the formation of complexing agents [61].

3.2.6. Effect of pH

The solution pH is an important control parameter for maintaining the effectiveness of the EF process. Several authors [20,27,62–66] have reported maximum efficiency in undivided cells with carbon-felt and gas diffusion (GDE) cathodes at pH 3.0, which is close to pH 2.8 where the maximum production of ·OH is expected from the Fenton's reaction. The pH was varied in the range of 2–7 and was found to be optimal around 3 with a total removal of CDM within 30 min. The pH was measured at the end of each test. No significant change was recorded between initial and final value of pH.

The low efficiency at lower pH (pH = 2) could be attributed to the stabilization of H_2O_2 which can form oxonium ion by solvating a proton. In the form of oxonium ion, hydrogen peroxide becomes electrophilic, leading to the enhancement of its stability and presumably to reduce substantial reactivity with ferrous ion as follows [67]:

$$H_2O_2 + H^+ \rightarrow H_3O_2^+ \tag{7}$$

It is remarkable from the Fig.14 that a significant degradation of CDM occurred at neutral pH (95.6 ± 1.7% within 60 min). However, only 32.7 ± 2.3% of NPOC was removed after 6 h of treatment, while it was 79.7 ± 1.7% at pH = 3 (Table 2).

3.2.7. Analysis of the degradation products of chlordimeform

In order to elucidate a plausible reaction pathway of CDM with hydroxyl radicals generated by the heterogeneous Electro-Fenton process, a LC–MS/MS analysis was conducted to follow the gradual disappearance of the insecticide molecule as well as the formation and the disappearance of the intermediate compounds during four hours of treatment (Fig.15). The corresponding experiment was conducted in
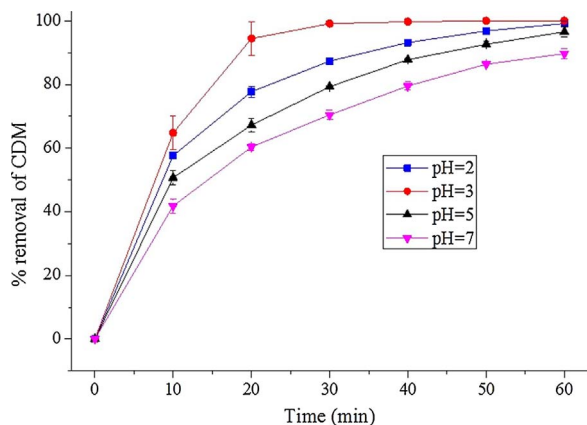

Fig. 14. Effect of the pH on CDM removal by Electro Fenton process using magnetic chitosan beads.

our optimal conditions. The identification was based on mass fragmentation values and by comparing the mass spectra to a database. The main compounds generated during the electro-Fenton treatment are described in Table 3. The evolution of the intermediate products formed during electrolysis is shown in Fig. 16. Degradation products of CDM were named CDM$_{1...3}$.

The oxidation of these derivatives with the electro-Fenton process led to the formation of short chain carboxylic acids which are the last by-products before mineralization; acetic acid (tr = 3.35 min), formic acid (tr = 4.02 min), succinic acid (tr = 15.23 min) and oxalic acid (tr = 22.14 min) were the main acids identified by ion chromatography in the final stage of CDM degradation; their retention times were compared with standard compounds. Time-courses of the carboxylic acid concentrations during treatment are given in Fig. 17. The fluctuation of acetic acid concentration can be explained by the high affinity in water between chitosan and this acid as reported by Shamov et al. [68].

The anions analysis by ion chromatography shows that the mineralization of CDM was accompanied by the conversion of its by-products into inorganic salts (data not shown). The CDM contains an atom of chlorine and two atoms of nitrogen. Therefore, the detection of inorganic salts such as chloride Cl^- and nitrates NO_3^- was expected. However no nitrite NO_2^- ions were produced. 25% of the expected amount of chloride ions from the target molecule was detected after 6 h of electrolysis. Nevertheless, a negligible amount of NO_3^- was quantified during the electro-Fenton treatment. This could be explained by the nitrogen transformation into ammonium ions NH_4^+. For this reason, an essay was conducted in our optimal experimental conditions for the removal of CDM to quantify the amount of ammonium ions during treatment. The determination of the NH_4^+ amount was performed by the Nessler spectrophotometric method. Results showed that after 6 h of electrolysis, the totality of the nitrogen present in the target molecule was transformed to ammonium ions.

The mechanism for CDM degradation by hydroxyl radical in water has not been yet discussed in the available literature. However, Shengmin Sun et al. [69], have studied this reaction in the atmosphere and they proposed several reaction channels including possible reactions initiated by hydroxyl radicals on the side chain and the benzene ring. Therefore, in Fig. 18 two plausible mineralization sequences are proposed for CDM removal during the electro-Fenton process on the basis of the identified intermediates including the two possibilities of reaction of hydroxyl radicals: one on the aromatic ring (**mechanism I**) and the other on the side chain (**mechanism II**). A thorough theoretical investigation [69] demonstrated that the reaction of the carbon-nitrogen double bond is the major channel, while the abstraction reaction from the benzene ring of CDM is the least competitive method.

In fact, the main proposed reaction was the electrophilic addition of a hydroxyl radical on the side chain (**mechanism II**) leading to the formation of chlortoluron. In a second step the removal of chloride atom would lead to the production of a substituted urea (1,1-dimethyl-3-(2-methylphenyl)urea). The next proposed step was the elimination of the C_2H_6N molecule, which would lead to the production of a substituted alcohol ([[(1-methylphenyl)amino]methanol). This is the final detected by-product prior to the ring-opening and the formation of short chain carboxylic acids.

3.2.8. Reusability of the catalyst

One of the most important advantages of heterogeneous catalysis is the reusability of the catalyst. To evaluate the stability of the catalytic activity of Fe_3O_4-Cs beads, the same catalyst was used successively four times. As can be seen, the catalyst can be reused four times without loss of its catalytic performance (Fig. 19). After four times of catalyst usage, only 5.4% decrease of the mineralization yield was found. From these, Fe_3O_4-CS beads were found to be a stable and reusable catalyst in the heterogeneous electro-Fenton process. The quantitative results of the amount of leached iron showed a zero iron concentration after 24 h of
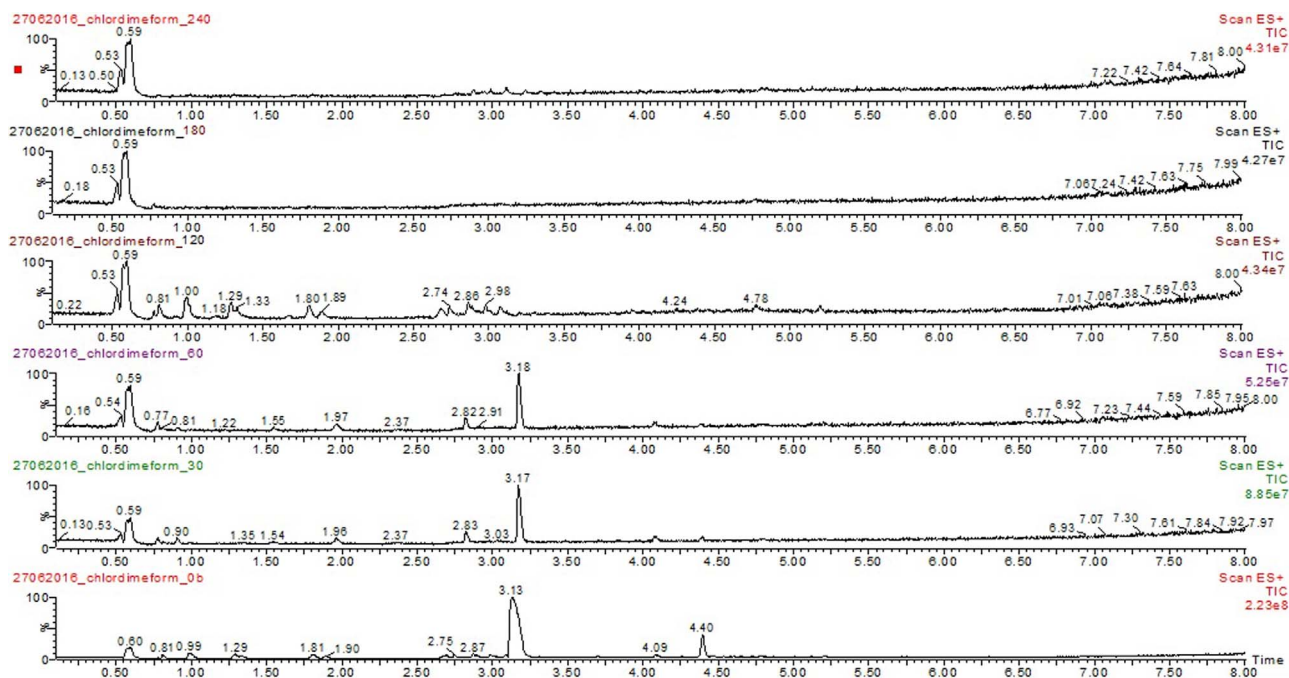
Fig. 15. LC–MS profiles of chlordimeform obtained during an heterogeneous electro-Fenton process with a working volume of 30 mL, Iimp = −5 mA, pH = 3 and [catalyst] = 0.5 g L^{-1}, $n_{Fe/massofcatalyst}$ = 0.104 ± 0.001 mmoL.

Table 3

LC–MS/MS identification of the chemical formula, retention time and main mass fragmentation values of identified chlordimeform (CDM) intermediates formed during the heterogeneous Electro-Fenton process.

Compound	Formula	tr (min)	M (g mol^{-1})	m/z (ES +)
CDM	$C_{10}H_{13}ClN_2$	3.13	196	197
CDM 1	$C_{10}H_{13}ClN_2O$	2.83	212	213
CDM 2	$C_{10}H_{14}N_2O$	0.90	178	179
CDM 3	$C_8H_{11}NO$	1.97	137	138

electrolysis time using the same catalyst. The negligible leaching of iron (inferior to the detection limit of the analysis technique estimated to 3.1 µmol L^{-1}) is due to the complex formation between amino groups of chitosan and iron as described previously. This is why the contribution of the leached iron in our heterogeneous system can be excluded and it can be affirmed that active catalytic sites are located on Fe_3O_4-Cs beads.

Furthermore, the molar ratio Fe^{2+}/Fe^{3+} is one of the most important operating factors that influence the characteristics of Fe_3O_4 nanoparticles, and it can affect the catalytic performance of our catalyst [70–72]. For this reason, the evolution of the molar ratio Fe^{2+}/Fe^{3+} was controlled during the preparation of Fe_3O_4-Cs beads and during the
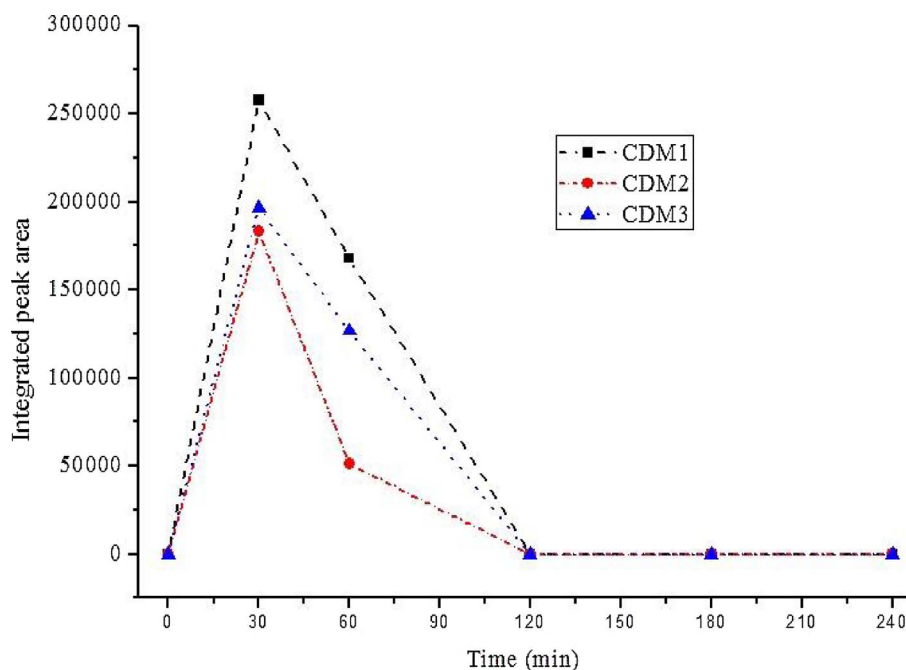
Fig. 16. Evolution of selected intermediates during the degradation of CDM under the conditions of Fig. 15.
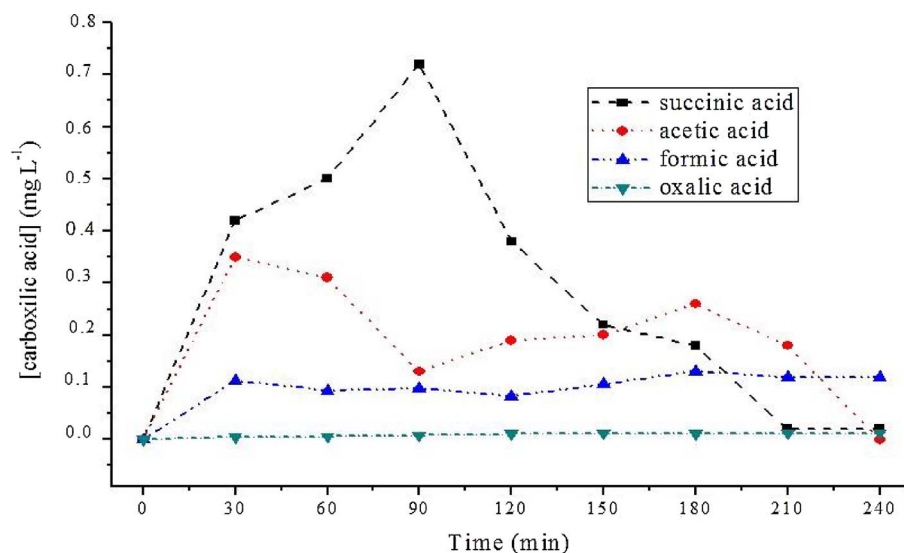
Fig. 17. Evolution of the formed carboxylic acids during the degradation of CDM under the conditions of Fig. 15.

electrolysis assays. The experimental Fe^{2+}/Fe^{3+} molar ratio being of the order of 0.517 ± 0.028, 0.481 ± 0.001 and 0.512 ± 0.015 in CS/iron salts gel solution (before the synthesis of Fe_3O_4) and in wet and dry Fe_3O_4-Cs beads (after the synthesis of Fe_3O_4) samples respectively (Table 4), namely close to the theoretical ratio of 0.5, proves that the synthesized magnetite product is pure enough [73]. During electrolysis, the molar ratio Fe^{2+}/Fe^{3+} in Fe_3O_4-Cs beads slightly decreased from initial value estimated to be 0.512 ± 0.015–0.422 ± 0.088 after 24 h of electrolysis, with a negligible decrease of its catalytic performance as mentioned previously. This can be explained by the instability of magnetite under oxidizing conditions (O_2, H_2O_2) where it is slowly oxidized to maghemite (γ-Fe_2O_3) which has the same spinal structure but contains only Fe(III) [72].

4. Conclusion

Magnetic chitosan beads (Fe_3O_4-Cs) were prepared in one step by a simple co-precepitation method. Fe_3O_4-Cs beads exhibited a catalytic performance for the degradation of CDM by an EF process with a high magnetic recovery. Our heterogeneous Fe_3O_4-Cs-EF system showed a higher performances compared to the conventional EF process using the same amount of iron. The effect of the amount of iron in chitosan beads
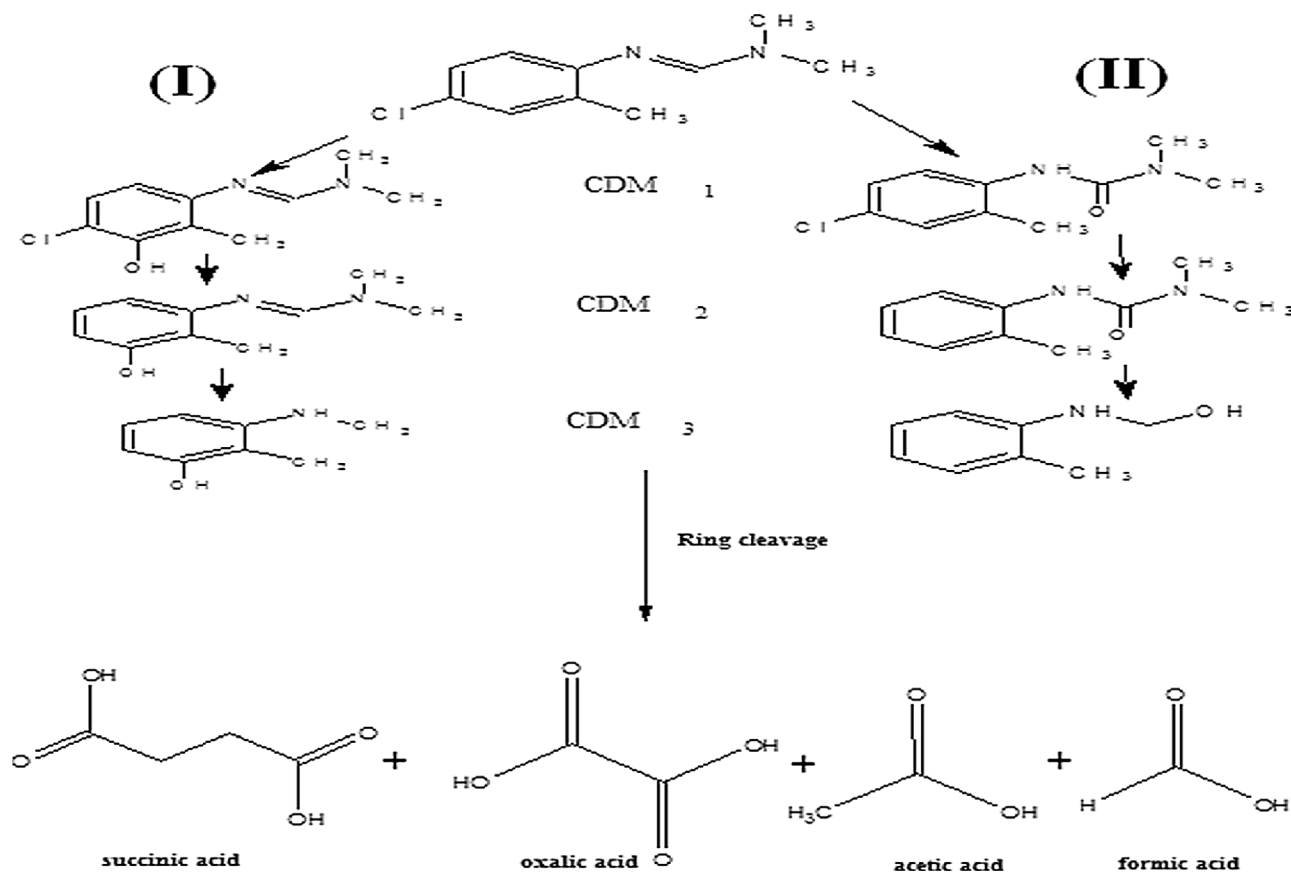

Fig. 18. Plausible degradation pathways of chlordimeform by the heterogeneous Electro-Fenton process.
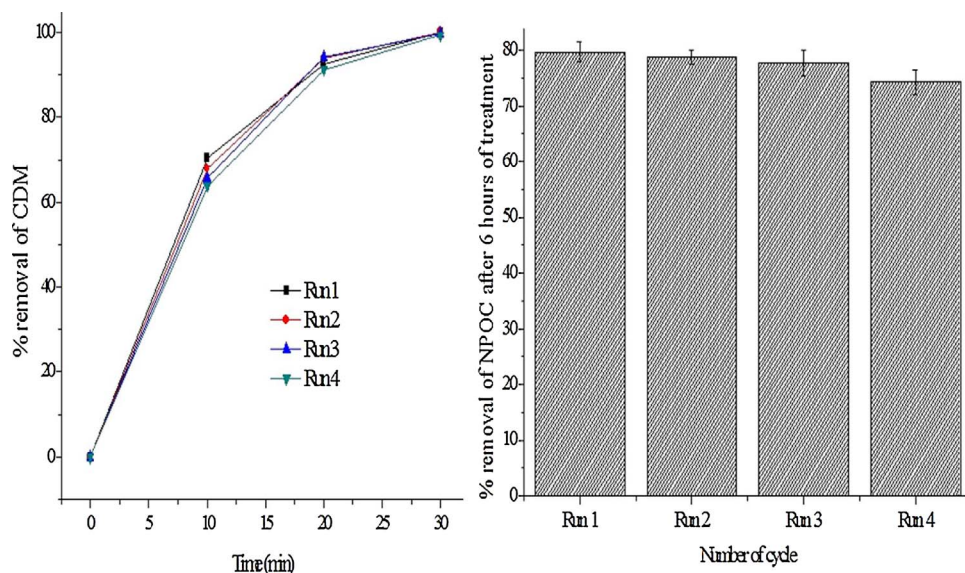
Table 4
Evolution of the Fe^{2+}/Fe^{3+} molar ratio.

Sample	Molar ratio Fe^{2+}/Fe^{3+}
Cs/iron salts gel solution	0.517 ± 0.028
Wet Fe_3O_4-Cs bead	0.481 ± 0.001
Dry Fe_3O_4-Cs bead	0.512 ± 0.015
After 6 hours of electrolysis	0.451 ± 0.039
After 12 hours of electrolysis	0.435 ± 0.114
After 18 hours of electrolysis	0.433 ± 0.078
After 24 hours of electrolysis	0.422 ± 0.088

was investigated. The optimal content was found to be 0.104 ± 0.001 mmol; complete CDM removal was observed within 30 min at an initial pH of 3.0, a cathodic current intensity of -5 mA and in the presence of $0.5\,g\,L^{-1}$ catalyst amount. In terms of organic carbon removal, about 80% mineralization yield was reached in the optimal conditions after 6 h of heterogeneous electro-Fenton treatment time. A kinetic analysis showed that the removal of CDM by Fe_3O_4-Cs beads followed a first-order kinetic model ($kapp = 0.160\,min^{-1}$). The intermediate by-products including short-chain carboxylic acids were identified and their evolution during the EF treatment was followed leading to the proposal of a degradation pathway for chlordimeform via hydroxyl radicals.

The recyclability of the catalyst was shown since it can be reused at least four times with a good catalytic performance. The main advantage which provides the stability of our catalyst is the combination between amino groups of chitosan and iron in the structure of Fe_3O_4-Cs that minimize the possibility of iron leaching and inhibits the aggregation of Fe_3O_4 nanoparticles which display a superparamagnetic property (Fe_3O_4 size $= 10.2$ nm), giving to our catalyst an additional stability limiting its loss of dispersibility in the absence of magnetic field. Furthermore, Fe_3O_4-Cs offers many advantages: low cost and toxicity, availability and environmentally friendly potential which make this catalyst a good candidate for industrial application in the field of water treatment.

Acknowledgement

References

[1] W. Zhang, F. Jiang, J. Ou, Global pesticide consumption and pollution: with China as a focus, Proc. Int. Acad. Ecol. Environ. Sci. 1 (2011) 125.
[2] D. Pimentel, Environmental and economic costs of the application of pesticides primarily in the United States, in: R. Peshin, A.K. Dhawan (Eds.), Integrated Pest Management: Innovation-Development Process, 1 Springer, Netherlandss, Dordrecht, 2009, pp. 89–111.
[3] J.A. Skinner, K.A. Lewis, K.S. Bardon, P. Tucker, J.A. Catt, B.J. Chambers, An overview of the environmental impact of agriculture in the U.K, J. Environ. Manage. 50 (1997) 111–128.
[4] M. Margni, D. Rossier, P. Crettaz, O. Jolliet, Life cycle impact assessment of pesticides on human health and ecosystems, Agriculture, Agric. Ecosyst. Environ. 93 (2002) 379–392.
[5] R. McKinlay, J.A. Plant, J.N.B. Bell, N. Voulvoulis, Endocrine disrupting pesticides: implications for risk assessment, Environ. Int. 34 (2008) 168–183.
[6] O. Osano, W. Admiraal, H.J.C. Klamer, D. Pastor, E.A.J. Bleeker, Comparative toxic and genotoxic effects of chloroacetanilides, formamidines and their degradation products on Vibrio fischeri and Chironomus riparius, Environ. Pollut. 119 (2002) 195–202.
[7] L.G. Costa, Costa, Chlordimeform A2 – Wexler, Philip, Encyclopedia of Toxicology, third edition, Academic Press, Oxford, 2014, pp. 849–850.
[8] A.E. Lund, G.K.W. Yim, D.L. Shankland, The cardiovascular toxicity of chlordimeform: a local anesthetic-like action, in: D.L. Shankland, R.M. Hollingworth, T. Smyth (Eds.), Pesticide and Venom Neurotoxicity, Springer, US, Boston, MA, 1978, pp. 171–177.
[9] W.K. Boyes, R.S. Dyer, Chlordimeform produces profound, selective, and transient changes in visual evoked potentials of hooded rats, Exp. Neurol. 86 (1984) 434–447.
[10] W.D. Thomas, G.K. Craig, N.H. Stacey, Effects of chlordimeform and its metabolite 4-chloro-o-toluidine on rat splenic T, B and tumoricidal effector cells, Immunopharmacology 19 (1990) 79–86.
[11] C.C. Davis, Environmental concerns about pesticide use in Philippine agriculture, Sci. Total Environ. 134 (1993) 293–306.
[12] R.E. Galt, Beyond the circle of poison: significant shifts in the global pesticide complex, 1976–2008, Global Environ. Change 18 (2008) 786–799.
[13] N. Wang, L. Shi, D. Kong, D. Cai, Y. Cao, Y. Liu, G. Pang, R. Yu, Accumulation levels and characteristics of some pesticides in human adipose tissue samples from Southeast China, Chemosphere 84 (2011) 964–971.
[14] X. Yang, J. Luo, Y. Duan, S. Li, C. Liu, Simultaneous analysis of multiple pesticide residues in minor fruits by ultrahigh-performance liquid chromatography/hybrid quadrupole time-of-fight mass spectrometry, Food Chem. 241 (2018) 188–198.
[15] E. Korta, A. Bakkali, L.A. Berrueta, B. Gallo, F. Vicente, V. Kilchenmann, S. Bogdanov, Study of acaricide stability in honey. Characterization of amitraz degradation products in honey and beeswax, J. Agric. Food Chem. 49 (2001) 5835–5842.
[16] X. Yi, L. Han, H. Yang, X. Fan, J. Zhu, D. Guo, [Determination of chlordimeform and its metabolite residues in honey using liquid chromatography-tandem mass spectrometry], Se pu = Chin. J. Chromatogr. 28 (2010) 649–653.
[17] C. Maqueda, E. Morillo, J.L. Pérez Rodríguez, A. Justo, Adsorption of chlordimeform by humic substances from different soils, Soil Sci. 150 (1990) 431–437.
[18] A. Babuponnusami, K. Muthukumar, A review on Fenton and improvements to the Fenton process for wastewater treatment, J. Environ. Chem. Eng. 2 (2014) 557–572.
[19] E. Neyens, J. Baeyens, A review of classic Fenton's peroxidation as an advanced oxidation technique, J. Hazard. Mater. 98 (2003) 33–50.

[20] C. Annabi, F. Fourcade, I. Soutrel, F. Geneste, D. Floner, N. Bellakhal, A. Amrane, Degradation of enoxacin antibiotic by the electro-Fenton process: optimization, biodegradability improvement and degradation mechanism, J. Environ. Manage. 165 (2016) 96–105.

[21] D. Mansour, F. Fourcade, I. Soutrel, D. Hauchard, N. Bellakhal, A. Amrane, Relevance of a combined process coupling electro-Fenton and biological treatment for the remediation of sulfamethazine solutions –application to an industrial pharmaceutical effluent, C.R. Chim. 18 (2015) 39–44.

[22] L. Ma, M. Zhou, G. Ren, W. Yang, L. Liang, A highly energy-efficient flow-through electro-Fenton process for organic pollutants degradation, Electrochim. Acta 200 (2016) 222–230.

[23] H. Roth, Y. Gendel, P. Buzatu, O. David, M. Wessling, Tubular carbon nanotube-based gas diffusion electrode removes persistent organic pollutants by a cyclic adsorption –electro-Fenton process, J. Hazard. Mater. 307 (2016) 1–6.

[24] K. Cruz-González, O. Torres-López, A. García-León, J.L. Guzmán-Mar, L.H. Reyes, A. Hernández-Ramírez, J.M. Peralta-Hernández, Determination of optimum operating parameters for Acid Yellow 36 decolorization by electro-Fenton process using BDD cathode, Chem. Eng. J. 160 (2010) 199–206.

[25] C.-T. Wang, J.-L. Hu, W.-L. Chou, Y.-M. Kuo, Removal of color from real dyeing wastewater by Electro-Fenton technology using a three-dimensional graphite cathode, J. Hazard. Mater. 152 (2008) 601–606.

[26] A. Wang, J. Qu, J. Ru, H. Liu, J. Ge, Mineralization of an azo dye Acid Red 14 by electro-Fenton's reagent using an activated carbon fiber cathode, Dyes Pigm. 65 (2005) 227–233.

[27] S.B. Hammouda, F. Fourcade, A. Assadi, I. Soutrel, A. Adhoum, L. Monser, Effective heterogeneous electro-Fenton process for the degradation of a malodorous compound, indole, using iron loaded alginate beads as a reusable catalyst, Appl. Catal. B: Environ. 182 (2016) 47–58.

[28] O. Iglesias, J. Gómez, M. Pazos, M.Á. Sanromán, Electro-Fenton oxidation of imidacloprid by Fe alginate gel beads, Appl. Catal. B: Environ. 144 (2014) 416–424.

[29] E.G. Garrido-Ramírez, J.F. Marco, N. Escalona, M.S. Ureta-Zañartu, Preparation and characterization of bimetallic Fe–Cu allophane nanoclays and their activity in the phenol oxidation by heterogeneous electro-Fenton reaction, Microporous Mesoporous Mater. 225 (2016) 303–311.

[30] C. Zhang, M. Zhou, X. Yu, L. Ma, F. Yu, Modified iron-carbon as heterogeneous electro-Fenton catalyst for organic pollutant degradation in near neutral pH condition: characterization, degradation activity and stability, Electrochim. Acta 160 (2015) 254–262.

[31] Z. Dong, X. Le, X. Li, W. Zhang, C. Dong, J. Ma, Silver nanoparticles immobilized on fibrous nano-silica as highly efficient and recyclable heterogeneous catalyst for reduction of 4-nitrophenol and 2-nitroaniline, Appl. Catal. B: Environ. 158–159 (2014) 129–135.

[32] S. Xing, Z. Zhou, Z. Ma, Y. Wu, Characterization and reactivity of Fe3O4/FeMnOx core/shell nanoparticles for methylene blue discoloration with H2O2, Appl. Catal. B: Environ. 107 (2011) 386–392.

[33] L. Hou, L. Wang, S. Royer, H. Zhang, Ultrasound-assisted heterogeneous Fenton-like degradation of tetracycline over a magnetite catalyst, J. Hazard. Mater. 302 (2016) 458–467.

[34] M. Minella, G. Marchetti, E. De Laurentiis, M. Malandrino, V. Maurino, C. Minero, D. Vione, K. Hanna, Photo-Fenton oxidation of phenol with magnetite as iron source, Appl. Catal. B: Environ. 154–155 (2014) 102–109.

[35] M. Mascolo, Y. Pei, T. Ring, Room temperature Co-Precipitation synthesis of magnetite nanoparticles in a large pH window with different bases, Materials 6 (2013) 5549.

[36] B. Hou, H. Han, S. Jia, H. Zhuang, P. Xu, D. Wang, Heterogeneous electro-Fenton oxidation of catechol catalyzed by nano-Fe3O4: kinetics with the Fermi's equation, J. Taiwan Inst. Chem. Eng. 56 (2015) 138–147.

[37] A. Kaushik, P.R. Solanki, A.A. Ansari, G. Sumana, S. Ahmad, B.D. Malhotra, Iron oxide-chitosan nanobiocomposite for urea sensor, Sens. Actuators, B 138 (2009) 572–580.

[38] R.J. White, R. Luque, V.L. Budarin, J.H. Clark, D.J. Macquarrie, Supported metal nanoparticles on porous materials. Methods and applications, Chem. Soc. Rev. 38 (2009) 481–494.

[39] Y. Lee, W. Lee, Degradation of trichloroethylene by Fe(II) chelated with cross-linked chitosan in a modified Fenton reaction, J. Hazard. Mater. 178 (2010) 187–193.

[40] E. Guibal, Heterogeneous catalysis on chitosan-based materials: a review, Prog. Polym. Sci. 30 (2005) 71–109.

[41] S. Sarkar, E. Guibal, F. Quignard, A.K. SenGupta, Polymer-supported metals and metal oxide nanoparticles: synthesis, characterization, and applications, J. Nanopart. Res. 14 (2012) 1–24.

[42] A. Elmagirbi, H. Sulistyarti, A. Atikah, Study of ascorbic acid as iron(III) reducing agent for spectrophotometric iron speciation, J. Pure App. Chem. Res. 1 (2012) 11–17.

[43] A.M. Cardenas-Peña, J. Ibanez, R. Vasquez-Medrano, Determination of the point of zero charge for electrocoagulation precipitates from an iron anode, Int. J. Electrochem. Sci. 7 (2012) 6142–6153.

[44] M. Islam, S. Md. Masum, M. Rahman, M. Ashraful Islam, A.A. Shaikh, S.K. Roy, Preparation of chitosan from shrimp shell and investigation of its properties, Int. J. Basic Appl. Sci. 11 (2011) 77–80.

[45] V.C.R. Massart, Synthese en milieu alcaline de magnetite colloidale, J. Chim. Phys. 84 (1987) 967.

[46] M.A.M. Gijs, Magnetic bead handling on-chip: new opportunities for analytical applications, Microfluid. Nanofluid. 1 (2004) 22–40.

[47] Y. Wang, B. Li, Y. Zhou, D. Jia, In situ mineralization of magnetite nanoparticles in chitosan hydrogel, Nanoscale Res. Lett. 4 (2009) 1041–1046.

[48] O. Stoilova, H. Penchev, T. Ruskov, I. Spirov, N. Manolova, I. Rashkov, One-pot preparation of magnetic chitosan beads, Bulgarian Chem. Commun. 40 (2008) 491–497.

[49] M. Lee, B.-Y. Chen, W. Den, Chitosan as a natural polymer for heterogeneous catalysts support: a short review on its applications, Appl. Sci. 5 (2015) 1272.

[50] X. Xiong, Y. Wang, W. Zou, J. Duan, Y. Chen, Preparation and characterization of magnetic chitosan microcapsules, J. Chem. 2013 (2013) 8.

[51] Y. Wang, B. Li, Y. Zhou, D. Jia, Chitosan-induced synthesis of magnetite nanoparticles via iron ions assembly, Polym. Adv. Technol. 19 (2008) 1256–1261.

[52] S. Arora Wahajuddin, Superparamagnetic iron oxide nanoparticles: magnetic nanoplatforms as drug carriers, Int. J. Nanomed. 7 (2012) 3445–3471.

[53] J. Brugnerotto, J. Lizardi, F.M. Goycoolea, W. Argüelles-Monal, J. Desbrières, M. Rinaudo, An infrared investigation in relation with chitin and chitosan characterization, Polymer 42 (2001) 3569–3580.

[54] L. Zhang, X. Zhu, S. Zheng, H. Sun, Photochemical preparation of magnetic chitosan beads for immobilization of pullulanase, Biochem. Eng. J. 46 (2009) 83–87.

[55] H.L. Ma, X.R. Qi, Y. Maitani, T. Nagai, Preparation and characterization of superparamagnetic iron oxide nanoparticles stabilized by alginate, Int. J. Pharm. 333 (2007) 177–186.

[56] Z. Abdeen, S.G. Mohammad, M.S. Mahmoud, Adsorption of Mn (II) ion on polyvinyl alcohol/chitosan dry blending from aqueous solution, Environmental Nanotechnology, Monit. Manage. 3 (2015) 1–9.

[57] L. Jin, R. Bai, Mechanisms of lead adsorption on chitosan/PVA hydrogel beads, Langmuir 18 (2002) 9765–9770.

[58] J. Paramo-Vargas, A.M.E. Camargo, S. Gutierrez-Granados, L.A. Godinez, J.M. Peralta-Hernandez, Applying electro-Fenton process as an alternative to a slaughterhouse effluent treatment, J. Electroanal. Chem. 754 (2015) 80–86.

[59] G. Santana-Martinez, G. Roa-Morales, E.M. del Campo, R. Romero, B.A. Frontana-Uribe, R. Natividad, Electro-Fenton and Electro-Fenton-like with in situ electrogeneration of H2O2 and catalyst applied to 4-chlorophenol mineralization, Electrochim. Acta 195 (2016) 246–256.

[60] Z. Qiang, J.-H. Chang, C.-P. Huang, Electrochemical generation of hydrogen peroxide from dissolved oxygen in acidic solutions, Water Res. 36 (2002) 85–94.

[61] M. Blanco, A. Martinez, A. Marcaide, E. Aranzabe, A. Aranzabe, Heterogeneous Fenton catalyst for the efficient removal of azo dyes in water, Am J. Anal. Chem. 5 (2014) 490–499.

[62] F. Sopaj, N. Oturan, J. Pinson, F. Podvorica, M.A. Oturan, Effect of the anode materials on the efficiency of the electro-Fenton process for the mineralization of the antibiotic sulfamethazine, Appl. Catal. B: Environ. 199 (2016) 331–341.

[63] D. Gümüş, F. Akbal, Comparison of fenton and electro-fenton processes for oxidation of phenol, Process Saf. Environ. Prot. 103 (2017) 252–258.

[64] H. Lin, N. Oturan, J. Wu, H. Zhang, M.A. Oturan, Cold incineration of sucralose in aqueous solution by electro-Fenton process, Sep. Purif. Technol. 173 (2017) 218–225.

[65] H. Lan, W. He, A. Wang, R. Liu, H. Liu, J. Qu, C.P. Huang, An activated carbon fiber cathode for the degradation of glyphosate in aqueous solutions by the Electro-Fenton mode: optimal operational conditions and the deposition of iron on cathode on electrode reusability, Water Res. 105 (2016) 575–582.

[66] M. Panizza, G. Cerisola, Electro-Fenton degradation of synthetic dyes, Water Res. 43 (2009) 339–344.

[67] H. Hassan, B. Hameed, Fenton-like oxidation of acid red 1 solutions UsingHeterogeneous catalyst based on ball clay, Int. J. Environ. Sci. Dev. 2 (2011) 218.

[68] M.V. Shamov, S. Bratskaya, V. Avramenko, Interaction of carboxylic acids with chitosan: Effect of pK and hydrocarbon chain length, J. Colloid Interface Sci. 249 (2002) 316–321.

[69] S. Sun, K. Zhang, Y. Lu, H. Zhang, Theoretical study on the reaction mechanism of chlordimeform with OH radicals, J. Mol. Model. 20 (2014) 1–10.

[70] S. Laurent, D. Forge, M. Port, A. Roch, C. Robic, L. Vander Elst, R.N. Muller, Magnetic iron oxide nanoparticles: synthesis, stabilization, vectorization, physicochemical characterizations, and biological applications, Chem. Rev. 108 (2008) 2064–2110.

[71] W. Jiang, K.-L. Lai, H. Hu, X.-B. Zeng, F. Lan, K.-X. Liu, Y. Wu, Z.-W. Gu, The effect of [Fe3 +]/[Fe2 +] molar ratio and iron salts concentration on the properties of superparamagnetic iron oxide nanoparticles in the water/ethanol/toluene system, J. Nanopart. Res. 13 (2011) 5135–5145.

[72] K. Rusevova, F.-D. Kopinke, A. Georgi, Nano-sized magnetic iron oxides as catalysts for heterogeneous Fenton-like reactions—influence of Fe(II)/Fe(III) ratio on catalytic performance, J. Hazard. Mater. 241-242 (2012) 433–440.

[73] M.C. Mascolo, Y. Pei, T.A. Ring, Room temperature Co-precipitation synthesis of magnetite nanoparticles in a large pH window with different bases, Materials 6 (2013) 5549–5567.